MITSUBISHI ELECTRIC RESEARCH LABORATORIES
http://www.merl.com

Model Predictive Control of Engine Speed During Vehicle Deceleration

Di Cairano, S.; Doering, J.; Kolmanovsky, I.V.; Hrovat, D.

TR2014-118 April 2014

Abstract

We consider the speed control of a spark ignition engine during vehicle deceleration. When the torque converter bypass clutch is open the engine speed needs to be kept close to the turbine speed to guarantee responsiveness of the vehicle for subsequent accelerations. However, to maintain vehicle drivability, undesired crossing between engine speed and turbine speed must not occur, despite the presence of significant torque disturbances. Hence, the engine speed during vehicle decelerations needs to be precisely controlled by feedback control, which has to coordinate airflow and spark timing and enforce several constraints including engine stall avoidance, combustion stability, and actuator limits. We develop a model predictive controller that manipulates airflow and spark to track the reference signal for engine speed while enforcing constraints, and synthesize it in the form of a feedback law. The controller is evaluated in simulations and in a vehicle, and it is shown to achieve a responsive and consistent deceleration and the potential for reducing fuel consumption.

IEEE Transactions on Technology

Model Predictive Control of Engine Speed during Vehicle Deceleration

S. Di Cairano, J. Doering, I.V. Kolmanovsky , D. Hrovat

***Abstract*—We consider the speed control of a spark ignition engine during vehicle deceleration. When the torque converter bypass clutch is open the engine speed needs to be kept close to the turbine speed to guarantee responsiveness of the vehicle for subsequent accelerations. However, to maintain vehicle drivability, undesired crossing between engine speed and turbine speed must not occur, despite the presence of significant torque disturbances. Hence, the engine speed during vehicle decelerations needs to be precisely controlled by feedback control, which has to coordinate airflow and spark timing and enforce several constraints including engine stall avoidance, combustion stability, and actuator limits. We develop a model predictive controller that manipulates airflow and spark to track the reference signal for engine speed while enforcing constraints, and synthesize it in the form of a feedback law. The controller is evaluated in simulations and in a vehicle, and it is shown to achieve a responsive and consistent deceleration and the potential for reducing fuel consumption.**

***Index Terms*—Engine control, Model predictive control, Automotive control systems, Constrained control.**

I. Introduction

In today's vehicles the powertrain control system is being continuously refined to improve fuel economy, emissions, safety, and drivability, thus making the vehicles more economical, sustainable, safe, and fun to drive. Drivability is the capability of the vehicle to be responsive and predictable to the driver's commands. While good drivability often goes unnoticed by the driver, poor drivability may lead to low driver confidence in the vehicle. Examples of poor drivability include, among others, lack of responsiveness, undesired responses to the driver commands and/or excessive vehicle jerk. Thus, a significant effort is devoted to refining the powertrain response by appropriate control system design and calibration. Due to multiple objectives and constraints, achieving good drivability can be complex and time consuming.

For vehicles equipped with standard automatic transmissions, the drivability effects are noticeable during vehicle deceleration. When the vehicle is decelerating and the torque converter bypass clutch is open, the torque provided to the vehicle is related to the turbine-engine speed ratio [1]–[4], the ratio between the speeds of the engine and of the torque converter turbine, which is connected to the gearbox input shaft. In order to obtain a consistent behavior, to maintain vehicle responsiveness, and to achieve high fuel economy, the engine speed during deceleration has to be precisely controlled. In spark ignition (SI) engines such control is achieved by manipulating the airflow and the spark timing, which, however, are subject to several constraints, including limits imposed by combustion stability and engine breathing.

Model predictive control (MPC) [5] systematically addresses the problem of achieving multiple objectives while enforcing constraints on vehicle inputs and states. Thus, it has the potential of significantly simplifying design and calibration of multivariable control systems. Furthermore, the execution of MPC controllers at high rate and with low computing power can be achieved by using the explicit MPC feedback law [6]. In this paper, we demonstrate the effectiveness of MPC in engine speed control during vehicle deceleration for vehicles equipped with standard automatic transmissions. MPC has been investigated for several automotive control applications, including engine control, driveline control, lateral vehicle dynamics control, and hybrid electric vehicle energy management [7]–[14]. See also the survey in [15]. Based on the authors' previous experience with idle speed control [16], MPC is a promising candidate for engine speed control during deceleration (engine deceleration control, for shortness).

The paper is organized as follows[1]. In Section II, we discuss the behavior of the powertrain during deceleration, and we introduce the engine deceleration control problem. In Section III we describe the physical model of the relevant dynamics during deceleration. Since the model is nonlinear, a control-oriented re-parametrization is proposed. In Section IV we design the MPC deceleration controller, which is synthesized as a feedback law for implementation in the engine control unit (ECU). In Section V, the controller is evaluated in simulations with disturbances and setpoint values recorded from real vehicle maneuvers. Then, in Section VI experimental tests spanning nominal and non-nominal deceleration conditions are reported. Conclusions are summarized in Section VII.

Notation: Real, positive real, nonnegative real, and integer, positive integer, nonnegative integer numbers are denoted by $\mathbb{R}$, $\mathbb{R}_+$, $\mathbb{R}_{0+}$, $\mathbb{Z}$, $\mathbb{Z}_+$, $\mathbb{Z}_{0+}$, respectively. For a continuous signal $a(t)$ sampled with period T_s, $a(k)$, $k \in \mathbb{Z}_{0+}$, denotes the value at the k^{th} sampling instant, $a(k) = a(kT_s)$, and $a(i|k)$, $i \in \mathbb{Z}_{0+}$ denotes the value $a(k+i)$ predicted based on data at kT_s. For a vector a, $[a]_i$ is the i^{th} component, and inequalities between vectors are intended as componentwise. In all figures the units are those introduced for the corresponding variables in the paper, unless otherwise indicated.

At the time of this research, S. Di Cairano was with Ford Research and Adv. Engineering, Dearborn, MI. He is now with Mitsubishi Electric Research Laboratories, Cambridge, MA, dicairano@ieee.org.

J. Doering and D. Hrovat are with Ford Research and Adv. Engineering, Dearborn, MI. jdoering,dhrovat@ford.com

I.V. Kolmanovsky is with Dept. of Aerospace Engineering, the University of Michigan, Ann Arbor, MI, ilya@umich.edu

[1]Preliminary studies related to this paper appeared in [17].

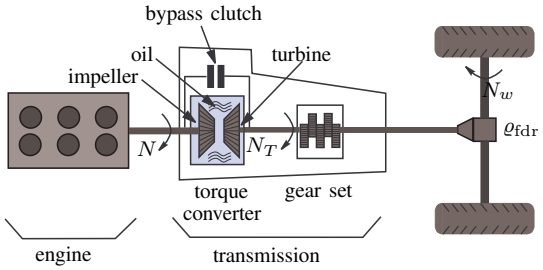

Fig. 1. Schematics of the powertrain components in the dynamical model used for engine deceleration control.

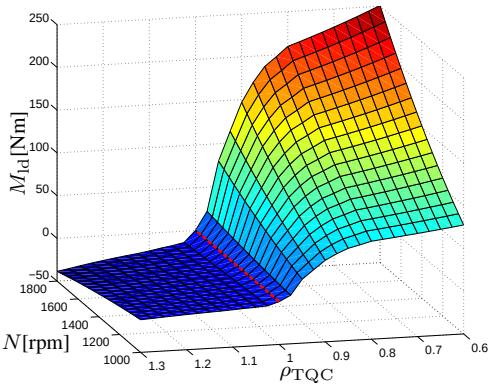

Fig. 2. Torque converter load on the engine $M_{\rm ld}$ as a function of the engine speed N and speed ratio $\rho_{\rm TQC} = N_T/N$. Segment with $\rho_{\rm TQC} = 1$ and $M_{\rm ld} = 0$ shown by the red (dash) line.

II. Engine Speed Control during Vehicle Deceleration

Figure 1 shows the schematic of the powertrain of a vehicle with standard automatic transmission. The engine and the transmission are connected through a torque converter, which shapes the torque transfer between the two. With some simplifications, the torque converter is composed of an impeller, rigidly connected to the crankshaft and thus rotating at the same speed as the engine, and of a turbine, rigidly connected to the transmission input shaft, that connects the torque converter to the gearbox. Turbine and impeller are immersed in oil, which realizes a hydraulic coupling between the two (the impeller spins the oil, which spins the turbine, and the other way around), hence allowing torque transfer between engine and transmission through the speed difference.

The engine speed dynamics are described by

$$J_e\dot{N} = (M_{\rm brk} - M_{\rm ld}), \tag{1}$$

where N[rpm] is the engine speed, J_e[rpm/(s·Nm)] is the lumped inertia of engine, flywheel, impeller and the oil rotating with it, $M_{\rm brk}$[Nm] is the engine brake torque (the net engine output torque) and $M_{\rm ld}$[Nm] is the load torque on the engine transmitted from the torque converter.

Neglecting the driveline dynamics, when the torque converter bypass clutch that directly connects the crankshaft to the transmission shaft is engaged and the transmission is "in-gear" (i.e., not shifting), the engine speed and turbine speed (N_T[rpm]) are equal, $N = N_T$, and the turbine speed is determined by the wheel speed, $N_T = \varrho_{\rm fdr}\varrho_{g_i}N_w$, where N_w[rpm] is the vehicle wheel speed, ϱ_{g_i}, $g_i = 1, \ldots, n_\varrho$ is the gear ratio, and $\varrho_{\rm fdr}$ is the final drive ratio. In these conditions and assuming a flat road, the load on the engine is a function of the wheel speed $M_{\rm ld} = \varrho_{\rm fdr}\varrho_{g_i}f_w(N_w)$, where f_w is a quadratic function [18].

When the torque converter bypass clutch is open, the engine speed and the turbine speed are in general not equal. In this case the load on the engine, i.e., on the crankshaft, $M_{\rm ld}$ is the torque transferred from the torque converter [1], [2], [4],

$$M_{\rm ld} = \frac{\mathrm{sign(N - N_T)} \cdot \max\{\mathrm{N, N_T}\}^2}{\mathcal{K}\left(\frac{N_T}{N}\right)^2}, \tag{2}$$

where $\mathcal{K}$ is a positive nonlinear function defined by the torque converter mechanical and hydrodynamical design. This function has maximum at 1, is monotonically increasing for arguments smaller than 1, and monotonically decreasing (although not symmetrically) for arguments larger than 1. For the vehicle used for experimental validation, a plot of the torque converter load on the engine $M_{\rm ld}$ as function of the engine speed N and of the torque converter speed ratio, $\rho_{\rm TQC} = N_T/N$ is shown in Figure 2. The curve for $\rho_{\rm TQC} > 1$ is significantly different from the one for $\rho_{\rm TQC} < 1$. This is due to the mechanical design of the torque converter [3], which maximizes the power transfer from the engine to the wheels, and minimizes the transfer from the wheels to the engine. In particular, for speed ratios larger than 1 the torque converter load changes are relatively small.

By (2), in the case of null external torques, when the engine speed is greater than the transmission speed, the turbine tends to accelerate and the impeller tends to decelerate, while when the engine speed is lower than the transmission speed, the opposite occurs. The hydraulic coupling introduces damping, hence smoothing the torque transfer from the engine to the driveline, and avoiding excessive jerk due to torque variations. The bypass clutch allows bypassing the hydraulic coupling for improved fuel economy, when damping is not needed (for instance in high gears).

A typical deceleration profile with brake application is shown in Figure 3, where different phases are highlighted. In the first phase (a), at high speed and in high gear, the torque converter bypass clutch is locked, so that $N = N_T$. In this phase usually there is no closed-loop control of the engine speed, and fuel injection may be shutoff. When the vehicle speed reduces and lower gears are engaged, the torque converter bypass clutch is opened (b) in order to avoid excessive jerk, and hence to maintain drivability. When the torque converter is open, the crankshaft and the transmission input shaft are coupled through the oil in the torque converter and the engine speed and the turbine speed become different. Initially, $N < N_T$, so that by (2) torque is transferred from the vehicle to the crankshaft, which increases the deceleration. At low gears and low vehicle speed (c), $N > N_T$ and, if the brakes are not applied, eventually the vehicle "creeps". If the brakes are applied, the vehicle speed and the turbine speed reach zero (d) and the engine speed is stabilized at idle.

When the torque converter is open (b–d), to provide good

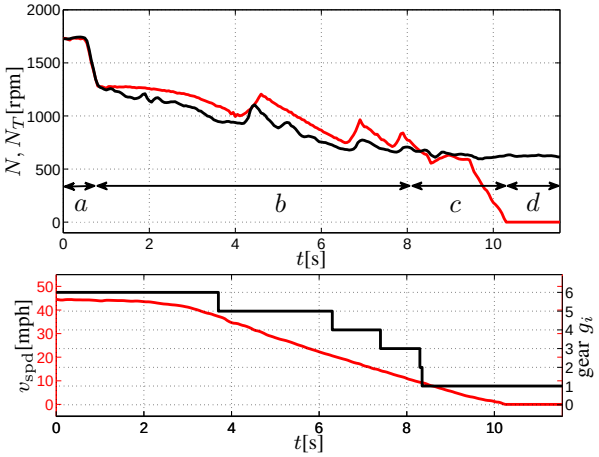

Fig. 3. Example of deceleration profile. Upper plot: Engine speed (black), turbine speed (red). Lower plot: Gear (black), vehicle speed (red), in mph.

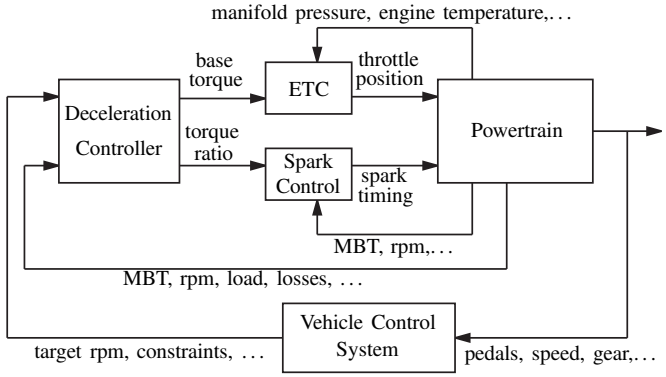

Fig. 4. Architecture for engine speed control during deceleration.

response to a driver's application of the accelerator pedal (the so-called "tip-in") while ensuring smooth and predictable vehicle deceleration without penalizing fuel consumption, the engine speed needs to be tightly controlled. If the engine speed is too low prior to a tip-in, it is difficult to provide smooth and responsive behavior since the engine has to be accelerated above transmission input shaft speed to provide positive torque to the wheels. If the engine speed is too high prior to a tip-in, the engine consumes more fuel than needed while decelerating. Also, the driveline has lash [19], and if the engine speed varies above and below transmission input shaft speed due to poor control, unintentional driveline lash crossings causing non-uniform deceleration and noise, vibration, and harshness (NVH) occur. Oscillations due to lash crossing may be felt by the driver as undesired accelerations that compromise the vehicle drivability. Thus, during deceleration, to provide fuel economy, powertrain responsiveness, and drive smoothness, precise feedback control of the engine speed is needed. Since the modification of the engine torque through the airflow is subject to delays and gas dynamics, a *spark torque reserve* is created for feedback control by advancing the spark timing from the optimal ignition timing. In this way, when disturbances occur, torque modifications can be achieved rapidly (in both directions) by manipulating the spark timing. However, the authority of the spark reserve is limited and it depends on the current engine airflow.

A well known speed control problem in automotive is Idle Speed Control (ISC) [20]. In ISC the engine speed is regulated to a constant setpoint using throttle (or bypass valve, in older engines) and spark timing, while rejecting disturbances caused for instance by air-conditioning and power steering pump load. Since the setpoint remains mostly constant, ISC operates in very specific, and almost stationary, engine operating conditions. The challenges in ISC are the time delay in the airpath and the reduced and varying authority of the spark actuation. Several control strategies have been proposed for ISC, see [20] and the references therein. Recently in [16], the authors have proposed an idle speed controller based on MPC that was experimentally shown to improve closed-loop robustness and to reduce the need for spark reserve, thus resulting in a more efficient engine operation.

While similar in terms of manipulated and controlled variables, engine speed control during deceleration is significantly more challenging than ISC, since the controller operates across several engine operating conditions, i.e., speeds and loads. The controller has to track various reference profiles generated by the vehicle control system according to the type of deceleration (braking, coasting, creeping, etc.). Some reference profiles can be rapidly changing (e.g., during braking), while others may be almost constant (e.g., during creeping). In all these conditions the controller must track the reference profile with small error (e.g., less than 50rpm), to provide a smooth and predictable deceleration (i.e., consistent in repeated maneuvers), and to maintain vehicle responsiveness to subsequent accelerations while avoiding undesired lash crossing events. The engine deceleration controller needs to counteract the disturbances that affect the idle controller. In addition it has to regulate the engine speed after a gear-shift, to engage from transient conditions, and to respond to reference profiles changing with rates that may not be achievable.

The architecture for engine speed control during deceleration is shown in Figure 4. The deceleration controller receives the powertrain state (engine speed, torque, etc.) from the vehicle sensors and estimators, and the desired engine speed and constraints from the vehicle control system. The controller commands the *base torque*, the maximum achievable indicated torque for the current airflow, and the torque ratio, the percentage of the base torque that is actually produced through spark modulation. The commanded base torque and the torque ratio are achieved by electronic throttle control and spark timing control implemented in lower level control functions that may exploit additional powertrain state variables, such as maximum brake torque (MBT) ignition angle [21], engine temperature, manifold pressure, etc. By this architecture, the engine deceleration control is decoupled from the actuator control, and hence the complexity of control design is reduced, and the resulting control system is modular.

Remark 1: In today's SI engines the air-to-fuel ratio is

tightly controlled to stoichiometry to maintain efficiency of the three-way catalyst which reduces emissions [22], and, as a consequence, it is not a manipulated variable for the engine deceleration control. Also, since it is tightly controlled to a constant value, the impact of air-to-fuel ratio fluctuations on the engine speed dynamics can be neglected [16].

The deceleration controller needs also to enforce constraints on state and control variables. The airflow cannot decrease below a minimum value, otherwise the combustion becomes unstable [21]. Similarly, an upper bound on the airflow has to be enforced, due to engine breathing conditions. Both these bounds vary significantly during deceleration. The torque ratio achieved by spark timing is also limited. Finally, the engine speed must be maintained above a given threshold designed conservatively to avoid engine stalls [16].

The design of classical controllers (e.g., PID-based) that achieve all these requirements can be cumbersome due to the need for selecting an appropriate logic to coordinate the control channels and to enforce saturation and anti-windup for dealing with the constraints. This may result in long development and calibration time and sub-optimal performance. The MPC approach proposed in this paper allows to obtain a controller that (optimally) coordinates the commands, while enforcing constraints by design.

III. Further Powertrain Modeling Details

Next, we model in greater details the powertrain dynamics that are relevant for engine speed control during deceleration. The engine brake torque in (1) is

$$M_{\rm brk} = M_{\rm ind} - M_{\rm ls}, \tag{3}$$

where $M_{\rm ind}$[Nm] is the engine indicated torque and $M_{\rm ls}$[Nm] are the torque losses due to pumping, friction, and accessory load. $M_{\rm ls}$ can be modelled as a complicated function of engine speed, ambient pressure and intake manifold pressure ($p_{\rm amb}$[Pa], $p_{\rm man}$[Pa]), engine temperature ($T_{\rm eng}$[K]) and accessory load ($M_{\rm acc}$[Nm]),

$$M_{\rm ls} = f_{\rm ls}(N, T_{\rm eng}, p_{\rm man}, p_{\rm amb}) + M_{\rm acc}.$$

Assuming stoichiometric operation according to Remark 1, the indicated torque is related to the torque ratio, $\kappa_{\rm spk} \in [0,1]$, and to the base torque, $M_{\rm air}$[Nm], by

$$M_{\rm ind} = \kappa_{\rm spk} M_{\rm air}. \tag{4}$$

The torque ratio is controlled by modulating spark timing σ[deg] (expressed as degrees with respect to top dead center) for the current engine speed and mass cylinder airflow $w_{\rm air}$[kg/s], $\kappa_{\rm spk} = f_\sigma(\sigma, w_{\rm air}, N)$, where $\kappa_{\rm spk} = 1$ for maximum brake torque spark timing ($\sigma = \sigma_{\rm MBT}(N, w_{\rm air})$). A commonly used form of f_σ is discussed in [16], [23], and the references therein. By (1), (2), (3), (4) we obtain

$$\dot N = \frac{1}{J_e}(\kappa_{\rm spk} M_{\rm air} - M_{\rm ls} - M_{\rm ld}). \tag{5}$$

Several variables in (5) are subject to operating constraints. The base torque is limited to the range,

$$M_{\rm air}^{\rm min}(t) \le M_{\rm air}(t) \le M_{\rm air}^{\rm max}(t), \tag{6}$$

where the lower bound $M_{\rm air}^{\rm min}(t)$ varies with time, and is imposed to avoid combustion instability (e.g., misfires) that occurs when too little air is trapped in the cylinder. In (6), the time-varying upper bound $M_{\rm air}^{\rm max}(t)$ reflects the maximum achievable torque, due to current engine operating conditions and operational requirements in terms of emissions, drivability, and NVH. Both $M_{\rm air}^{\rm min}$, $M_{\rm air}^{\rm max}$ mainly depend on engine speed, load, and temperature. Similarly, the torque ratio is lower and upper bounded due to emissions, combustion stability, and physical limitations,

$$0 \le \kappa_{\rm spk}^{\rm min} \le \kappa_{\rm spk} \le \kappa_{\rm spk}^{\rm max} \le 1\ , \tag{7}$$

where $\kappa_{\rm spk}^{\rm min}$, $\kappa_{\rm spk}^{\rm max}$ are constant during deceleration.

In the torque domain, the control variables for engine speed regulation are the commanded base torque $\hat M_{\rm air}$[Nm] and the commanded torque ratio $\hat\kappa_{\rm spk}$. The action of $\hat M_{\rm air}$, $\hat\kappa_{\rm spk}$ is not instantaneous due to the presence of dynamics and time delays. The base torque generation process is subject to the combustion time delay $\delta_{\rm air}$[s] which is usually assumed to be 360 crank angle degrees, and hence its time duration [2] depends on the engine speed, $\delta_{\rm air} = \frac{60}{N}$. Furthermore, due to manifold filling dynamics, the base torque generation is subject to a first order lag with a time constant $\tau_{\rm air}$[s]. Thus, the dynamics from commanded to generated base torque are

$$\dot M_{\rm air}(t) = \frac{1}{\tau_{\rm air}}(-M_{\rm air}(t) + \hat M_{\rm air}(t - \delta_{\rm air}(t))). \tag{8}$$

Remark 2: From physics, the torque dynamics are the manifold filling dynamics, a first order lag, followed by a combustion time delay. Here, by linearity, we use an equivalent model with input time delay.

The effect of the torque ratio actuation via spark is also subject to a delay due to the discrete firing of the cylinders, which, for a 6 cylinders vehicle, is 120 crank angle degrees, i.e., $\delta_{\rm spk} = \frac{60}{3N}$. Hence,

$$\kappa_{\rm spk}(t) = \hat\kappa_{\rm spk}(t - \delta_{\rm spk}). \tag{9}$$

By collecting (2), (5)–(9), the complete dynamical model is

$$\begin{aligned}
\dot N(t) &= \frac{1}{J_e}(\hat\kappa_{\rm spk}(t-\delta_{\rm spk}) M_{\rm air}(t) \\
&\qquad - M_{\rm ls}(t) - M_{\rm ld}(t)), && \text{(10a)}\\
\dot M_{\rm air}(t) &= \frac{1}{\tau_{\rm air}}(-M_{\rm air}(t) + \hat M_{\rm air}(t - \delta_{\rm air}(t))), && \text{(10b)}\\
M_{\rm ld}(t) &= \frac{\mathrm{sign}(\mathrm{N} - \mathrm{N_T}) \cdot \max\{\mathrm{N}, \mathrm{N_T}\}^2}{\mathcal{K}\left(\frac{N_T}{N}\right)^2}, && \text{(10c)}\\
& M_{\rm air}^{\rm min}(t) \le M_{\rm air}(t) \le M_{\rm air}^{\rm max}(t), && \text{(10d)}\\
& \kappa_{\rm spk}^{\rm min} \le \hat\kappa_{\rm spk}(t) \le \kappa_{\rm spk}^{\rm max}, && \text{(10e)}
\end{aligned}$$

where the state variables are the engine speed N, the base torque $M_{\rm air}$, and the past commands for base torque and spark torque ratio along the time delay windows, $\hat M_{\rm air}(\tau)$, $\tau \in [t - \delta_{\rm air}, t)$ and $\hat\kappa_{\rm spk}(\tau)$, $\tau \in [t - \delta_{\rm spk}, t)$; the control inputs are the commanded base torque $\hat M_{\rm air}$ and the commanded

[2] Alternatively crank angle can be used as independent variable, resulting in a constant delay model. However, other aspects of the dynamics become significantly more complicated [24].

spark torque ratio $\hat{\kappa}_{\rm spk}$; and the measured disturbances are the turbine speed N_T and the torque losses $M_{\rm ls}$. In (10) the torque losses dynamics have been neglected, since their changes are small and/or slow in the operating conditions of interest.

Remark 3: The powertrain dynamics in (10) are connected to the longitudinal vehicle dynamics. A simple longitudinal vehicle dynamics model is

$$J_v\dot{N}_w = \varrho_{g_i}\varrho_{\rm fdr}M_T - M_{\rm rl}, \tag{11}$$

where J_v[Nm/(rpm/s)] is the vehicle inertia at the wheels, M_T[Nm] is the output torque of the torque converter and $M_{\rm rl}$ is the road load. For zero road grade, the road load is a function of the vehicle speed only, $M_{\rm rl} = f_w(N_w)$. Based on (2), the torque converter output torque is a function of the engine and turbine speed, $M_{\rm T} = f_{is}(N, N_T)$. When the transmission is in-gear, $N_w = N_T/(\varrho_{g_i}\varrho_{fdr})$. By substituting into (11),

$$J_v\dot{N}_w = \varrho_{g_i}\varrho_{\rm fdr}f_{is}(N, \varrho_{g_i}\varrho_{fdr}N_w) - f_w(N_w), \tag{12}$$

and hence the vehicle speed depends on the engine speed. Due to the torque converter design [3], when the engine speed is below the turbine speed, the torque transmitted though the converter is small and does not change significantly with the speed ratio (see Figure 3). Hence, during deceleration the engine speed can be modulated with limited impact on the vehicle deceleration profile. However, precise engine speed control is needed to maintain high fuel economy and vehicle responsiveness while avoiding lash crossings which cause NVH and reduced drivability.

A. Control-oriented parametrization

It is difficult to use model (10) for MPC design since it is nonlinear and subject to (variable) time delays. A re-parametrization can be performed to remove the nonlinearity as described by the following proposition.

Proposition 1: Consider

$$z(t) = x(t)u(t), \tag{13a}$$
$$u^{\min} \le u(t) \le u^{\max}, \tag{13b}$$

where $x, u, z \in \mathbb{R}$, and

$$\zeta(t) = v(t), \tag{14a}$$
$$u^{\min}x(t) \le v(t) \le u^{\max}x(t), \tag{14b}$$

where $\zeta, v \in \mathbb{R}$. Let $x : [t_0, t_f] \to \mathbb{R}_+$. Then for all $u : [t_0, t_f] \to \mathbb{R}$ satisfying (13b) for all $t \in [t_0, t_f]$ there exist a unique $v : [t_0, t_f] \to \mathbb{R}$ satisfying (14b) for all $t \in [t_0, t_f]$ such that $\zeta(t) = z(t)$ for all $t \in [t_0, t_f]$.

The proof of Proposition 1 is immediate. One obtains (14) from (13) by introducing $v \in \mathbb{R}$ as $v(t) = u(t)x(t)$. The result follows from the fact that $x(t) > 0$ for all $t \in [t_0, t_f]$ and hence the transformation is invertible. Note also that when $x(t) = 0$, $v(t) = 0$, but still $\zeta(t) = z(t)$ independently of $u(t)$.

In (14) we have reformulated a bilinear relation subject to bounds, as a linear relation subject to linear constraints. For applying the result in Proposition 1 to (10), we notice that $M_{\rm air}(t) > 0$ for all t, and define a nominal torque ratio $\bar{\kappa}_{\rm spk}$,

$$\kappa_{\rm spk}(t) = \bar{\kappa}_{\rm spk} + \Delta\kappa_{\rm spk}(t), \tag{15a}$$
$$\Delta\kappa_{\rm spk}^{\min} \le \Delta\kappa_{\rm spk}(t) \le \Delta\kappa_{\rm spk}^{\max}, \tag{15b}$$

where $\Delta\kappa_{\rm spk}^{\min} = \kappa_{\rm spk}^{\min} - \bar{\kappa}_{\rm spk}$, and $\Delta\kappa_{\rm spk}^{\max} = \kappa_{\rm spk}^{\max} - \bar{\kappa}_{\rm spk}$. By substituting (15) into (10a),

$$\dot{N}(t) = \frac{1}{J_e}(\bar{\kappa}_{\rm spk}M_{\rm air}(t) + M_{\rm spk}(t) - M_{\rm ls}(t) - M_{\rm ld}(t)),$$

where $\bar{\kappa}_{\rm spk}$ is the indicated torque obtained from the current base torque and the nominal torque ratio, and $M_{\rm spk}(t) = \Delta\kappa_{\rm spk}(t)M_{\rm air}(t)$ is the additional torque obtained by applying a torque ratio different from nominal. The box constraints on torque ratio difference from nominal (15b) become linear constraints between torque ratio and base torque,

$$\Delta\kappa_{\rm spk}^{\min}M_{\rm air}(t) \le M_{\rm spk}(t) \le \Delta\kappa_{\rm spk}^{\max}M_{\rm air}(t). \tag{16}$$

In the new parametrization the control variables are the commanded engine indicated torque for spark at nominal value, $u_{\rm air}$, and the commanded additional torque, $u_{\rm spk}$, from modulating spark timing around nominal value. Thus from (10), (15), (16), we obtain

$$\dot{N}(t) = \frac{1}{J_e}(\bar{\kappa}_{\rm spk}M_{\rm air}(t) + u_{\rm spk}(t-\delta_{\rm spk}) - M_{\rm ls}(t) - M_{\rm ld}(t)), \tag{17a}$$
$$\dot{M}_{\rm air}(t) = \frac{1}{\tau_{\rm air}}(-M_{\rm air}(t) + u_{\rm air}(t-\delta_{\rm air}(t))), \tag{17b}$$
$$M_{\rm ld}(t) = \frac{\max\{N(t), N_T(t)\}^2\text{sign}(\text{N(t)} - \text{N}_\text{T}\text{(t)})}{\mathcal{K}\left(\frac{N_T(t)}{N(t)}\right)^2}, \tag{17c}$$
$$M_{\rm air}^{\min}(t) \le M_{\rm air}(t) \le M_{\rm air}^{\max}(t), \tag{17d}$$
$$\Delta\kappa^{\min}M_{\rm air}(t) \le u_{\rm spk}(t-\delta_{\rm spk}) \le \Delta\kappa^{\max}\ M_{\rm air}(t), \tag{17e}$$

which is a constrained system subject to linear constraints with controls $u_{\rm air}$, $u_{\rm spk}$, states N, $M_{\rm air}$, and past commands along the delay periods, $u_{\rm air}(\tau)$, $\tau \in [t-\delta_{\rm air}, t)$, $u_{\rm spk}(\tau)$, $\tau \in [t-\delta_{\rm spk}, t)$, and measured disturbances $M_{\rm ls}$, N_T.

Remark 4: For most control strategies (14) does not simplify the design, because constraints involving multiple states (or states and inputs) are difficult to enforce. However, MPC has the capability of enforcing such constraints by design, and hence it can control the bound constrained bilinear relation (13) though controlling the linearly constrained linear relation (14).

IV. Model Predictive Control Design

The advantage of model (17) with respect to (10) is that, except for (17c), the dynamics are linear, subject to linear constraints and time delays. As a result, (17) can be used in a linear-quadratic model predictive control algorithm.

A. Prediction model formulation

In order to simplify the computations, we remove (17c) and consider $M_{\rm ld}$, which is estimated by the vehicle control system via (17c), as a measured disturbance. The variable delays in (17b) are approximated as constant multiples of the sampling period T_s, i.e., $\delta_{\rm air}(t) = T_s\bar{\delta}_{\rm air}$, for all $t \ge 0$, and $\bar{\delta}_{\rm air} \in \mathbb{Z}_{0+}$. Similarly, the fixed spark-timing delay is approximated as a multiple of the sampling period, $\delta_{\rm spk} = T_s\bar{\delta}_{\rm spk}$. Although better results can be achieved by gain scheduling multiple controllers based on different delay durations, we

have verified that, during deceleration, this approximation does not significantly limit the performance. On the other hand, assuming constant delays reduces the amount of storage memory needed in the ECU.

Under these simplifications, (17) sampled with period T_s results in the discrete-time linear dynamics

$$x(k+1) = Ax(k) + Bv(k) + \Gamma w(k), \tag{18}$$

where $x = [N\ M_{\rm air}]'$, $v(k) = [u_{\rm air}(k-\bar{\delta}_{\rm air}))\ u_{\rm spk}(k-\bar{\delta}_{\rm spk})]'$, $w = [M_{\rm ld}\ M_{\rm ls}]'$. The model of the input time delay is

$$\begin{aligned} x_\delta(k+1) &= A_\delta x_\delta(k) + B_\delta u(k), & (19a)\\ v(k) &= C_\delta x_\delta(k), & (19b)\end{aligned}$$

where x_δ is of the size of the number of delays in the system, in this case $x_\delta \in \mathbb{R}^{\delta_{\rm spk}+\delta_{\rm air}}$, $u = [u_{\rm air}\ u_{\rm spk}]' \in \mathbb{R}^2$, and A_δ, B_δ, C_δ implement a delay buffer [16].

The value of the measured disturbances is known/estimated by the vehicle control system, but their dynamics are not known. Hence they are modeled as constant in prediction,

$$w(k+1) = w(k). \tag{20}$$

This approximation is based on the assumption that the measured disturbances changes are small and/or slow with respect to the other variables. The receding horizon operation of the MPC controller further compensates for such an approximation. At any control cycle the value of the measured disturbances is acquired and used to initialize the constant prediction model (20) for prediction along the MPC horizon. At the subsequent step, the MPC controller acquires the new value of the measured disturbances and adjusts the control sequence based on such an updated value.

Thus, the prediction model from (18), (19), (20) is

$$x(k+1) = A_f x_f(k) + B_f u_f(k), \tag{21}$$

where $x_f \in \mathbb{R}^{4+\delta_{\rm spk}+\delta_{\rm air}}$, $x_f = [x'\ x'_\delta\ w']'$, and $u_f = u \in \mathbb{R}^2$.

In order to obtain the full prediction model for MPC design we need to further extend (21) to enforce the control design specification for the engine deceleration controller.

For a constant reference and constant load, the spark timing should return to the nominal value at steady state in order to maintain a torque reserve against future disturbances. Thus, the spark torque $M_{\rm spk}$ should decrease to zero, while the base torque $M_{\rm air}$ should converge to an (unknown) steady state. As a consequence, we formulate $u_{\rm air}$ in incremental form, and add an integrator on $u_{\rm spk}$, to be used in the cost function

$$\begin{aligned} \xi_u(k+1) &= \xi_u(k) + T_s u_{\rm spk}(k), & (22a)\\ x_u(k+1) &= x_u(k) + \Delta u_{\rm air}(k), & (22b)\\ u_{\rm air}(k) &= x_u(k) + \Delta u_{\rm air}(k), & (22c)\end{aligned}$$

where $\Delta u_{\rm air}$ is the input variation from previous step and ξ_u is the integral of the spark torque. Removing $\Delta u_{\rm air}(k)$ in (22c) models an additional step of delay on the base torque.

Since we want to obtain a controller that rejects constant disturbances and achieves offset-free tracking of constant references, we add a model for the engine speed reference r[rpm] and an integrator on the tracking error

$$\begin{aligned} r(k+1) &= r(k) + T_s \Delta r(k), & (23a)\\ \Delta r(k+1) &= \Delta r(k), & (23b)\\ \xi_r(k+1) &= \xi_r(k) + T_s(N(k) - r(k)), & (23c)\end{aligned}$$

where Δr[rpm/s] is the gradient of the reference, which is known in this application and assumed constant in prediction, and ξ_r is the integral of the tracking error.

Additional ancillary equations relates to the torque upper and lower bounds in (17d). These values change depending on the engine operating conditions, and even if their current values are known, their future values are difficult to predict. Thus, we treat them as constant in prediction,

$$\begin{aligned} M_{\rm air}^{\min}(k+1) &= M_{\rm air}^{\min}(k), & (24a)\\ M_{\rm air}^{\max} r(k+1) &= M_{\rm air}^{\max}(k). & (24b)\end{aligned}$$

As for the measured disturbances (20), the bounds in (24) are updated at every control cycle with values computed by the vehicle control system, resulting in time-varying base torque bounds.

Equations (22), (23), (24) together with (21) define the full prediction model used in MPC

$$x_p(k+1) = A_p x(k) + B_p u_p(k), \tag{25}$$

where $x_p = [x'_f\ x'_u\ r\ \Delta r\ \xi_u\ \xi_r\ M_{\rm air}^{\min}\ M_{\rm air}^{\max}]'$, $x_p \in \mathbb{R}^{11+\delta_{\rm spk}+\delta_{\rm air}}$.

B. Cost function and constraints

The MPC engine deceleration controller is calibrated by appropriately shaping the cost function. The control objective is to track the engine speed reference with zero steady-state offset for constant references and constant disturbances. Also, at steady state the spark timing has to return to its setpoint. These objectives are encoded in the cost function

$$\begin{aligned} J = \sum_{i=0}^{h-1} &(N(i) - r(i))^2 + \rho_r \xi_r(i)^2 + \rho_u \xi_u(i)^2 \\ &+ \rho_s M_{\rm spk}^2 + \rho_a \Delta u_{\rm air}^2, \end{aligned} \tag{26}$$

where $h \in \mathbb{Z}_+$ is the MPC prediction horizon, i.e., the time interval along which the cost function is integrated based on the prediction of the system dynamics, and ρ_r, ρ_u, ρ_s, ρ_a are positive weighting coefficients.

The remaining operating specifications, combustion stability, limits on base torque and spark timing, and minimum engine speed are enforced by the constraints

$$\begin{aligned} y_p(k) &= Cx_p(k), & (27a)\\ y^{\min} \le\ y_p(k) &\le y^{\max}, & (27b)\end{aligned}$$

where $[y_p]_1 = M_{\rm air} - M_{\rm air}^{\max}$ and $[y_p]_2 = M_{\rm air} - M_{\rm air}^{\min}$ enforce (17d), $[y_p]_3 = [C_\delta x_\delta]_2 - \Delta\kappa^{\max} M_{\rm air}$, $[y_p]_4 = [C_\delta x_\delta]_2 - \Delta\kappa^{\min} M_{\rm air}$, enforce (17e), and $[y_p]_5 = N$ enforces $N \ge \underline{N}$ to avoid engine stalls. In (27b), upper and lower bounds are assumed plus and minus infinity, respectively, for unbounded quantities.

C. Controller design and synthesis

The MPC finite horizon optimal control problem is formulated based on (25), (26), (27),

$$\min_{U_p(k)} \quad \sum_{i=0}^{h-1} x_p(i|k)'Qx_p(i|k) + u_p(i|k)'Ru_p(i|k) \tag{28a}$$

$$\text{s.t.} \quad x_p(i+1|k) = A_p x_p(i|k) + B_p u_p(i|k) \tag{28b}$$

$$y_p(i+1|k) = Cx_p(i|k) \tag{28c}$$

$$y_i^{\min} \leq y_p(i|k) \leq y_i^{\max}, i = \bar{\delta}_{\text{spk}}, \ldots, h_c + \bar{\delta}_{\text{air}} \tag{28d}$$

$$u_p(i|k) = 0, i = h_u, \ldots, h-1 \tag{28e}$$

$$x_p(0|k) = x_p(k)\ , \tag{28f}$$

where $U_p(k) = (u_p(0|k), \ldots, u_p(h-1|k))$, and $h_u \in \mathbb{Z}_+$ is the control horizon, the number of free control moves available for the controller along the prediction horizon. In (28d) the bounds change depending on the time step to generalize the constraint horizon for system with multiple time delays. It is not possible to enforce the constraints from the beginning of the horizon, since the controller cannot modify the system response in an interval shorter than the shortest input time delay. Hence, after defining $h_c \in \mathbb{Z}_+$, we enforce the constraints on minimum and maximum base torque ($[y]_1(i|k)$, $[y]_2(i|k)$) for $i = \bar{\delta}_{\text{air}}, \ldots, \bar{\delta}_{\text{air}} + h_c$, the constraints on minimum and maximum torque from spark modulation ($[y]_3(i|k)$, $[y]_4(i|k)$) for $i = \bar{\delta}_{\text{spk}}, \ldots, \bar{\delta}_{\text{spk}} + h_c$, and the constraint on engine speed $[y]_5(i|k)$ for $i = \bar{\delta}_{\text{spk}}, \ldots, \bar{\delta}_{\text{air}} + h_c$, where $\delta_{\text{spk}} < \delta_{\text{air}}$, according to Section III. In (28) we set $[y_i^{\max}]_j = -[y_i^{\min}]_j = \infty$ for the steps i when the constraints are not enforced.

At every step $k \in \mathbb{Z}_{0+}$, the model predictive control algorithm executes the following: (i) builds the current state vector $x_p(k)$ from the current estimated and measured signals; (ii) solves finite horizon optimal control problem (28) initialized from $x_p(k)$; (iii) computes the command for the base torque and for the torque ratio from the optimal input sequence $U_p^*(k)$ and the current state $x_p(k)$ by

$$\hat{\kappa}_{\text{spk}}(k) \quad = \quad \frac{u^*_{\text{spk}}(0|k)}{M_{\text{air}}(k + \bar{\delta}_{\text{spk}})}, \tag{29a}$$

$$\hat{M}_{\text{air}}(k) \quad = \quad x_u(k) + \Delta u^*_{\text{air}}(k). \tag{29b}$$

In (29a), the correct computation of the spark ratio command requires the prediction of the base torque to compensate for the delay in the spark control channel. Since $\bar{\delta}_{\text{spk}} < \bar{\delta}_{\text{air}}$, $M_{\text{air}}(k + \bar{\delta}_{\text{spk}})$ in (29a) can be computed from the current state and past inputs by integrating the system dynamics.

In order to meet the stringent chronometric and memory requirements of automotive ECUs, we use multiparametric programming [6] to synthesize the explicit MPC feedback law as the piecewise affine function

$$U_p^*(k) \quad = \quad F_{j(k)} x_p(k) + G_{j(k)} \tag{30a}$$

$$j(k) \in \{1, \ldots, s\} \quad : \quad H_{j(k)} x_p(k) \leq K_{j(k)}\ , \tag{30b}$$

where (30b) defines the polyhedral region partitions, s is the total number of regions, and (30a) assigns an affine expression to each region. The explicit synthesis of the MPC controller presents several advantages in terms of functionality and integration process. Specifically, there is no need to solve the optimization problem at every control cycle, but only to evaluate (30). Also, the worst case number of operations to execute per control cycle, as well as the required memory, can be precisely computed, and hence feasibility of the implementation of the controller in a given computing platform can be verified. Finally, a closed-loop system model is obtained from (25), (30),

$$x_p(k+1) \quad = \quad (A + B\Phi F_j)x_p(k) + \Phi G_j \tag{31a}$$

$$j: \quad H_j x_p(k) \leq K_j, \tag{31b}$$

where $\Phi = [I\ 0]$, $\Phi \in \mathbb{R}^{2 \times 2h}$, selects the first command of the optimal control sequence. System (31) is a piecewise affine system whose local and global stability and robustness margins can be analyzed using tools and methods available in the literature [16], [25].

V. Controller Evaluation in Simulations

The MPC controller designed in Section IV is implemented with a sampling period $T_s = 16$ms and horizons $h_p = 20$, $h_c = 3$, $h_u = 3$. Based on the intermediate speed $N = 1200$rpm, the numbers of delay samples in torque and spark actuation channels have been set to $\bar{\delta}_{\text{air}} = 3$, $\bar{\delta}_{\text{spk}} = 1$, i.e., 48ms and 16ms, respectively. We set the lower bound on the engine speed as $\underline{N} = 400$rpm. The sampling period is the same as the one of the production controller in the ECU, which is based on the tradeoff between performance and chronometric requirements. The choice of the prediction horizon is based on the bandwidth of the dominant system dynamics, which, for engine speeds in the interval of 1000-1500rpm is in the range of $3 - 5$Hz. Finally, the control and constraint horizons are chosen to tradeoff the explicit controller performance versus complexity. For the chosen values, the explicit MPC controller (30) results in $s = 78$ regions for a total of 469 inequalities. Using the techniques in [25], we have verified that the closed-loop system (31) is locally asymptotically stable around the equilibrium. We have verified that the robustness margin guarantees stability for at least 0.011s of additional delay in the base torque dynamics, which is sufficient for the operating conditions of interest. Thus, the controller design is slightly conservative at high engine speed. Such conservativeness may be reduced if more advanced stability analysis methods for systems with variable delay are used [26].

For evaluating the proposed control design, a simulation model based on (10) has been implemented, where the parameters have been identified from the prototype vehicle used later for experimental validation. The reference and measured disturbances for the simulations, r, N_T, M_{ls} in (10), have been recorded in the vehicle while executing a baseline controller.

Remark 5: The turbine speed (and as a consequence the load on the engine) and the torque losses are affected by the engine speed. The engine speed profile obtained by MPC is (obviously) not exactly the same as the engine speed in the data recording experiments. As a consequence the measured disturbances used for simulations are not exactly those that the controller will experience. However, during the data recording, the engine speed is maintained close to the reference by the

baseline controller, and if the same occurs in simulation, the engine speed profiles in simulation and in the experiment are similar. Hence, the approximations of $M_{\rm ld}$ and $M_{\rm ls}$ are reasonable, given also that the changes of $M_{\rm ld}$ and $M_{\rm ls}$ in the operating conditions occurring during deceleration are relatively small and slow.

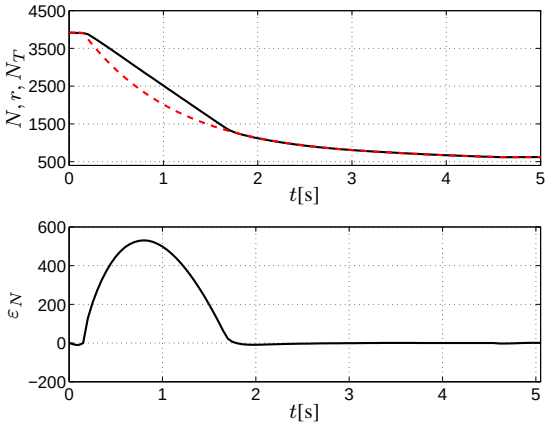

(a) Upper plot: engine speed (solid), reference (dash). Lower plot: engine speed tracking error.

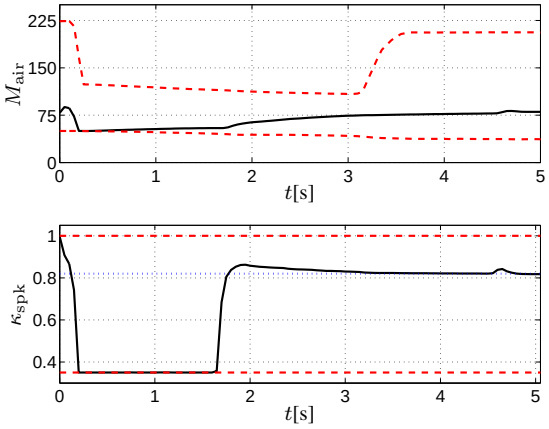

(b) Upper plot: base torque (solid), torque constraints (dash). Lower plot: torque ratio by spark (solid), constraints (dash), setpoint (dot).

Fig. 5. Simulation of deceleration in neutral with stationary vehicle.

In order to verify the capability of the controller of tracking a rapidly changing reference, in Figure 5 we show the deceleration from the maximum (limiter) engine speed to idle speed when the vehicle is in neutral and not moving. In this test the engine speed reference decreases by 3000rpm in less than 2s, and at the same time the load on the crankshaft is very small since the powertrain is in neutral, i.e., $N_T \approx N$. The controller cannot track the moving reference with 0 offset in the initial part of the deceleration. This is due to the small load on the crankshaft, and to the combustion stability constraint which imposes a lower bound on the commanded torque. However, the controller is able to enforce all the constraints and to "softly land" on the reference without undershoot.

In Figure 6 we show the simulation of a deceleration from high gear (6^{th}, in this case) while the vehicle is moving. The vehicle is decelerated with the application of brakes causing downshifts to 1^{st} gear (the last is 3^{rd}–1^{st}), which are easily

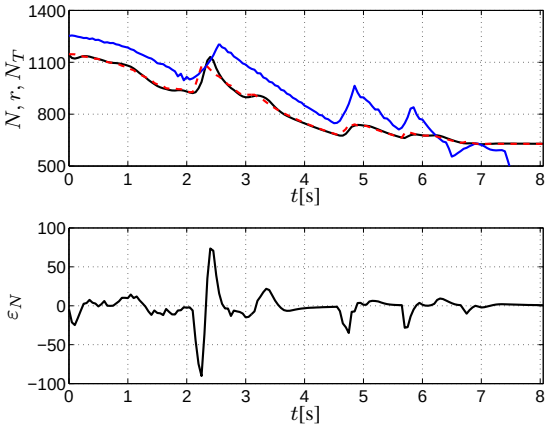

(a) Upper plot: engine speed (solid), reference (dash), turbine speed (blue). Lower plot: engine speed tracking error.

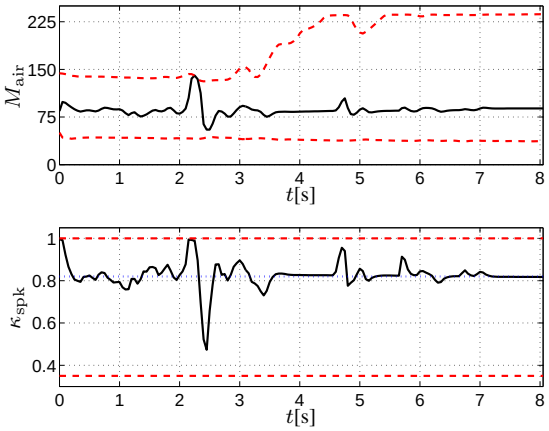

(b) Upper plot: base torque (solid), torque constraints (dash). Lower plot: torque ratio by spark (solid), constraints (dash), setpoint (dot).

Fig. 6. Simulation of rapid deceleration with downshifts with moving vehicle.

noticeable by the sudden increase in the turbine speed. The reference profile to be tracked is designed for achieving good drivability and is generated by a separate function in the vehicle control system. All the constraints are satisfied, and the reference trajectory is tracked with a small error. Compared to the simulated deceleration in neutral in Figure 5, the reference engine speed decelerates at a slower rate, and there is a higher load on the crankshaft, which helps the deceleration. Since when the engine speed is larger than the turbine speed the engine is driving the wheels, while in the other case the wheels are driving the engine, the controller has to maintain the engine speed on the desired side relative to the turbine speed to avoid unintended lash crossings in the driveline. In the simulation no undesired lash crossings occur.

VI. Experimental Results

The control strategy is synthesized in C-code for implementation in a dSPACE DS1401 rapid prototyping unit. The test platform is a FWD production vehicle equipped with a 3.7L V6 engine and a 6 speed standard automatic transmission. The controller in the rapid prototyping unit receives the current targets (reference and constraint bounds) and the

measurements/estimates for the plant variables from the ECU, constructs the prediction model state vector, evaluates the MPC feedback law, computes the actuators commands, and sends them to the ECU which actuates them by the existing actuator drivers and lower level controllers. The communication between rapid prototyping unit and ECU takes place via CAN, which introduces additional delays that will not be present when the control system is entirely implemented in the target platform, and hence not included in the prediction model. We have verified that the impact of the additional delays is appreciable only when the controller is initially engaged, causing a slightly larger initial tracking error.

While executed in the rapid prototyping unit for the simplicity of development, the controller computational requirements have been evaluated for implementation in the automotive powertrain control unit. The worst case number of atomic operations (scalar sums, multiplications, and comparisons to 0) is less than 10^6 per second, which amounts to less than 1% of the CPU capabilities. The total ROM size (mostly calibration memory) is about 10kB, and only 6 additional variables have to be stored in RAM, the commands along the delay windows in (19) and the integrators in (22), (23). In extensive experimental tests we have verified that the average CPU capabilities used are less than 10% of the worst case, and that the storage memory usage can be reduced by a factor of 4 by simple data compression.

A. Experiments in stationary and driving conditions

In Figure 7 we show the experimental results for the deceleration in neutral. The behavior is qualitatively similar to the one observed in the simulation in Figure 5, where it is not possible to closely track the reference speed due to the low load and to the combustion stability constraint (6). We also note that due to the way the engine maps are identified, in these operating conditions the engine torque actuation error (the difference between requested and delivered torque) may be significant (up to 30%). The proposed controller provides soft landing on the reference also in the experiments, with negligible undershoot. We have repeated the test with the transmission in drive and the vehicle kept stationary by braking, see Figure 8. In this case, there is a large difference between the engine speed and the turbine speed ($N_T = 0$), and hence there is a larger load on the crankshaft, so that the engine speed can track the reference also during the transient. The error transients when the controller is activated ($t = 4$s, 12s, 20s) are in part caused by the CAN induced time-delay.

Next, we show the results of a test where the vehicle was driven along an appropriately designed test course. The course involves different types of decelerations, including coastdowns, rapid decelerations using brakes, low speed creeping. As a further challenge, the test was executed with the air conditioning (AC) compressor engaged, where any error in the estimate of AC load introduces additional disturbances. The AC load during this test varied unpredictably between 5Nm and 15Nm. Figure 9 describes the scenario and highlights the different operating conditions that the test exercises. Some relevant maneuvers are discussed in details, next.

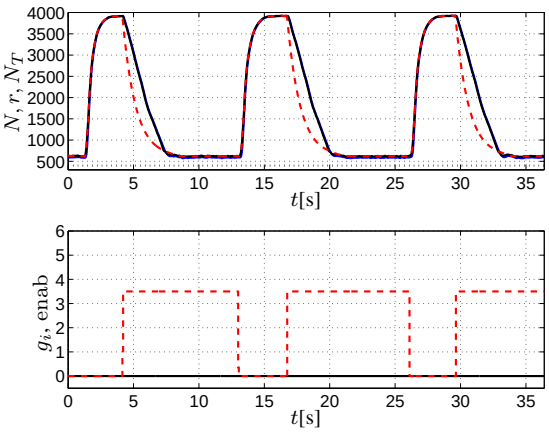

(a) Upper plot: engine speed (solid), reference (dash), engine speed constraint (dot). Lower plot: controller enabling signal (dash), gear (solid, 0 means neutral).

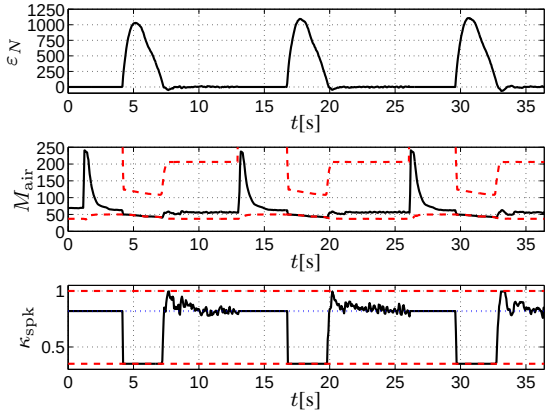

(b) Upper plot: tracking error (0 when inactive). Middle plot: base torque (solid), torque constraints (dash). Lower plot: torque ratio by spark (solid), constraints (dash), setpoint (dot).

Fig. 7. Experimental test of deceleration in neutral with stationary vehicle.

In Figure 10 we show a maneuver where the vehicle is creeping (Figure 3, phase c) in a roughly paved parking area, with a 2^{nd}–1^{st} downshift, where the $1^{\rm st}$ gear of the vehicle has an over-running one-way clutch. Due to the low speed and low torque, this is a critical maneuver since any small disturbance can be felt. However, the controller precisely tracks the desired deceleration profile also after the downshift, which involves a large change in the gear ratio.

In Figure 11 we show a coastdown without the application of brakes (until $t = 162$s) ending with several consecutive downshifts. Initially the torque converter is locked (Figure 3, phase a) and $N = N_T$. After the 6-5 downshift the torque converter is unlocked and closed-loop speed control begins (Figure 3, phase b). The controller follows the target speed profile, rejecting load disturbances (e.g., around $t = 143$s), which are due to, for instance, power steering and AC compressor load changes. During the downshifts the controller maintains the engine speed on the desired side of the turbine speed.

An aggressive deceleration while braking is shown in Figure 12, similar to the simulation in Figure 6. The powertrain goes through multiple downshifts and even in this case the MPC is able to always maintain the engine speed on the correct

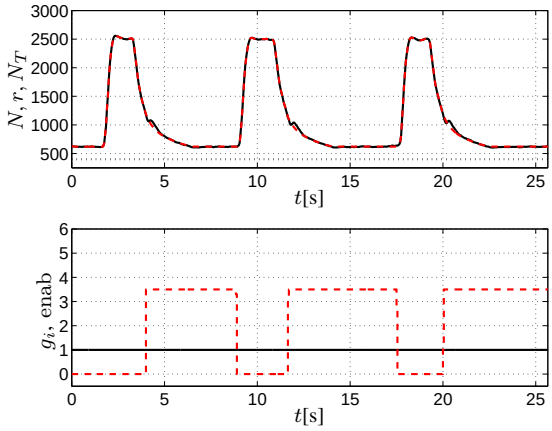

(a) Upper plot: engine speed (solid), reference (dash), engine speed constraint (dot). Lower plot: controller enabling signal (dash) gear (solid, 0 is neutral).

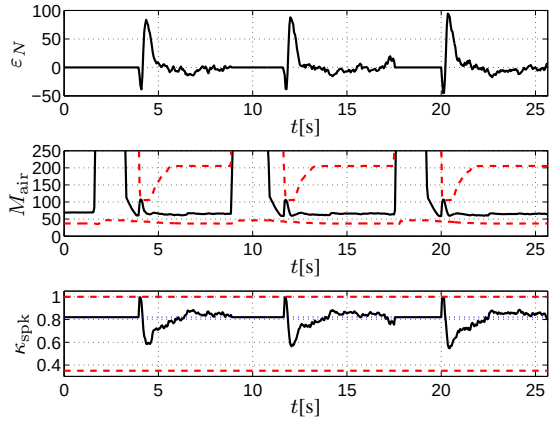

(b) Upper plot: tracking error (0 when inactive). Middle plot: base torque (solid), torque constraints (dash). Lower plot: torque ratio by spark (solid), constraints (dash), setpoint (dot).

Fig. 8. Experimental test of deceleration in drive with stationary vehicle.

side with respect to the turbine speed. The crossing between turbine speed and engine speed (Figure 3, b to c), which changes the sign of the load torque per (2), is well controlled ($t = 50.5$s), which results in the driver not experiencing a significant jerk or NVH.

B. Experiments in non-nominal and faulty conditions

The controller operation was verified also in the case of non-nominal and faulty conditions. One of such tests is reported in Figure 13, where the vehicle was stationary with the transmission in neutral and near idle speed (Figure 3, phase d), which, as discussed before, is a particularly challenging condition due to the limited load on the crankshaft, larger actuation errors, and longer delays. In the test, a disturbance ϑ_{d} is added to the commanded electronic throttle angle ϑ_{cmd}, simulating faults in the throttle. These cause large and sudden torque disturbances, since the base torque is different from what expected. During the test the throttle angle output disturbance is not corrected by any other control loop. In Figure 13(a) we see that the steady state throttle angle with the vehicle stationary in neutral is only slightly above 1deg. The disturbances are steps between

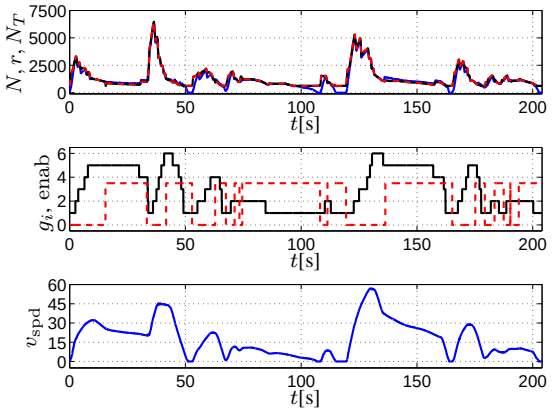

Fig. 9. Scenario of normal on road driving along a test course. Upper plot: engine speed (solid), reference (dash), turbine speed (blue). Middle plot: controller enabling signal (dash) gear (solid, 0 means neutral). Lower plot: vehicle speed [mph].

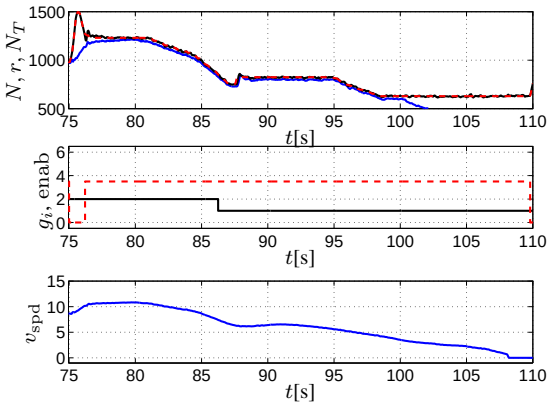

(a) Upper plot: engine speed (solid), reference (dash), turbine speed (blue). Middle plot: controller enabling signal (dash) gear (solid, 0 means neutral). Lower plot: vehicle speed [mph].

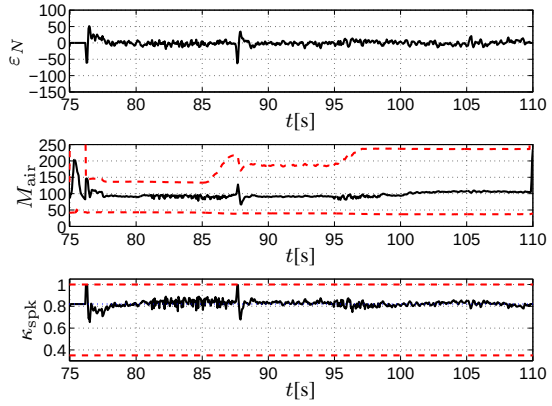

(b) Upper plot: tracking error (0 when inactive). Middle plot: base torque (solid), torque constraints (dash). Lower plot: torque ratio by spark (solid), constraints (dash), setpoint (dot).

Fig. 10. Experimental test of low speed maneuver (creeping).

-1deg and $+2$deg, causing large relative torque disturbances, since in this conditions the torque is approximately linearly proportional to the throttle angle. The controller is robust to these disturbances, rejecting them rapidly and enforcing the constraints.

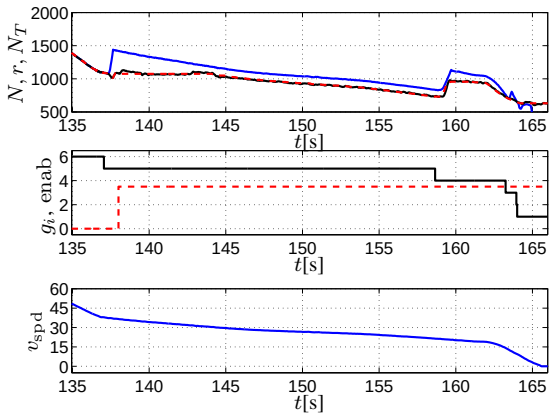

(a) Upper plot: engine speed (solid), reference (dash), turbine speed (blue). Middle plot: controller enabling signal (dash) gear (solid) 0 means neutral). Lower plot: vehicle speed [mph].

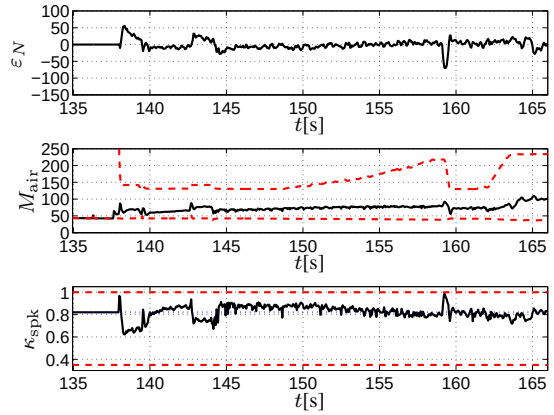

(b) Upper plot: tracking error (0 when inactive). Middle plot: base torque (solid), torque constraints (dash). Lower plot: torque ratio by spark (solid), constraints (dash), setpoint (dot).

Fig. 11. Experimental test of coastdown with downshifts without braking.

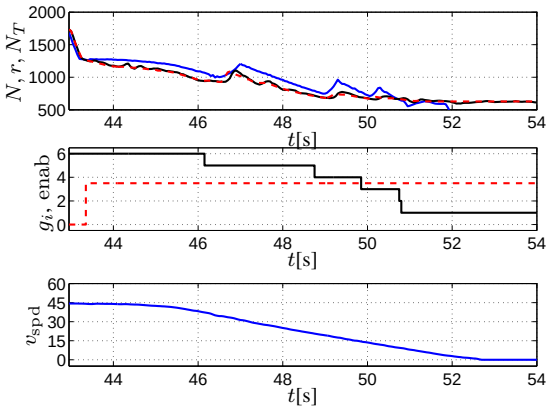

(a) Upper plot: engine speed (solid), reference (dash). Middle plot: controller enabling signal (dash) gear (solid, 0 means neutral). Lower plot: vehicle speed, [mph].

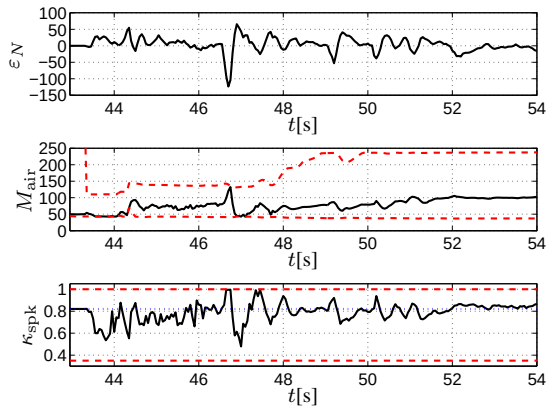

(b) Upper plot: tracking error (0 when inactive). Middle plot: base torque (solid), torque constraints (dash), turbine speed (blue). Lower plot: torque ratio by spark (solid), constraints (dash), setpoint (dot).

Fig. 12. Experimental test of rapid deceleration with downshifts while braking.

When the throttle angle disturbance increases from 0deg to 2deg ($t = 65$s) the controller cannot bring the spark back to the setpoint, since the steady state value of the commanded throttle angle would need to be negative, in the prediction model. However, the controller cannot command a negative base torque (i.e., a negative throttle angle) because it has to maintain the base torque above the combustion stability limit, and the disturbance on the throttle angle is unknown even to the function that computes such limit. Thus, MPC uses the spark -including at steady state- to compensate for the disturbance. Finally, when the throttle angle disturbance decreases from 2deg to 0deg the lower bound on the engine speed is briefly violated ($t = 88$s). The maximum violation is approximately 50rpm and lasts less than 250ms. However, since the limit on the engine speed is designed slightly conservatively and implemented as a soft constraint, the controller continues operating and rapidly recovers by commanding a rapid increase of the base torque request, which, when delivered, is modulated by the spark ($t = 89$s).

C. Performance assessment

We have compared the proposed control strategy to a baseline controller and assessed the difference in performance. The baseline controller uses a gain-scheduled PID design with feedforward and antiwindup which outputs the desired brake torque. The feedforward is computed to compensate the torque load ($M_{\rm ld}$) and losses ($M_{\rm ls}$) estimated from the same engine maps used by MPC. The brake torque request computed by the control strategy is allocated to engine torque and spark torque ratio by an appropriate algorithm. This also guarantees that an appropriate spark torque reserve is maintained by implementing a form of mid-ranging [27] on the base torque. The baseline controller is a robust and effective strategy, yet, since it does not optimally account for the dynamic interactions between the control inputs in the presence of constraints, its performance can be improved. Also, the design of the saturation and anti-windup is rather cumbersome due to the many constraints, resulting in a complex control logic. An immediate benefit of MPC is that the constraints are dealt with by design in a systematic way. In terms of performance the MPC controller has shown improvements in terms of

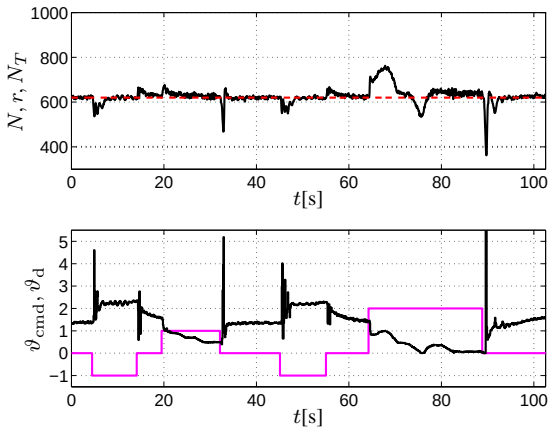

(a) Upper plot: engine speed (solid), reference (dash), engine speed constraint (dot). Lower plot: commanded throttle angle and additive throttle angle disturbance (in degrees).

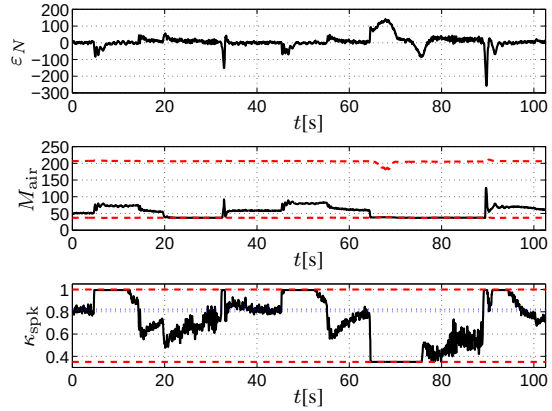

(b) Upper plot: tracking error (0 when inactive). Middle plot: base torque (solid), torque constraints (dash). Lower plot: torque ratio by spark (solid), constraints (dash), setpoint (dot).

Fig. 13. Experimental test of robustness to throttle faults.

tracking and robustness. Quantitatively, in the deceleration tests the settling time was reduced on average by 11% and by 62% in neutral (Figure 7) and drive (Figure 8), respectively. The performance improvement in neutral is less pronounced because all the actuators are saturated for most of the test, and hence there are no degrees of freedom to optimize. Along the whole driving scenario (Figure 9) the RMS tracking error is reduced by 16%. Also, we have observed that the torque ratio is on average 1.15% higher when using the MPC controller, due to the more precise tracking of the engine speed reference which allows to bring the torque ratio to its nominal value more rapidly. As a consequence, the engine runs closer to MBT, and hence more efficiently, reducing the fuel consumption by 1.32%. While a decisive improvement of the engine efficiency was not the primary objective, we note that this can be accomplished by increasing the spark ratio nominal value and consequently tightening the constraints on torque from spark modulation. Preliminary tests have shown that in this way the fuel economy during deceleration can be improved by more than 3% while keeping the same tracking performance as the baseline controller.

VII. Conclusions

We have proposed a systematic design for engine speed control during vehicle deceleration, when the torque converter is open. The multivariable constrained controller must keep the engine speed close to the turbine speed to maintain vehicle responsiveness, yet it should avoid crossing the lash to minimize disturbances on the driveline and degraded drivability. By re-parametrizing the powertrain dynamics to eliminate a multiplicative nonlinearity, we have implemented a feedback controller based on linear-quadratic MPC which enforces the powertrain constraints. In experimental tests the controller has been shown to achieve improved tracking performance and fuel economy as compared to a baseline strategy. In terms of its computational footprint, the controller is adequate for implementation in a production ECU.

Acknowledgments

The authors acknowledge C. Cox and S. Szwabowski of Ford Motor Co., for support with the test vehicle, and Dr. D. Yanakiev of Ford Motor Co., for useful discussions.

References

[1] A. Kotwicki, "Dynamic models for torque converter equipped vehicles," in *Proc. SAE World Congress*, Detroit, MI, 1982, paper N. 820393.

[2] D. Hrovat and W. Tobler, "Bond graph modeling and computer simulation of automotive torque converters," *J. of the Franklin Institute*, vol. 319, no. 1/2, pp. 93–114, 1985.

[3] S. Shin, H. Chang, and M. Athavale, "Numerical investigation of the pump flow in an automotive torque converter," in *Proc. SAE World Congress*, Detroit, MI, 1999, paper N. 1999-01-1056.

[4] J. Deur, J. Asgari, D. Hrovat, and P. Kovač, "Modeling and analysis of automatic transmission engagement dynamics-linear case," *J. of Dynamic Systems, Meas. and Control*, vol. 128, pp. 263–277, 2006.

[5] C. Garcia, D. Prett, and M. Morari, "Model predictive control: theory and practice–a survey," *Automatica(Oxford)*, vol. 25, no. 3, pp. 335–348, 1989.

[6] A. Bemporad, M. Morari, V. Dua, and E. Pistikopoulos, "The explicit linear quadratic regulator for constrained systems," *Automatica*, vol. 38, no. 1, pp. 3–20, 2002.

[7] N. Giorgetti, G. Ripaccioli, A. Bemporad, I. Kolmanovsky, and D. Hrovat, "Hybrid Model Predictive Control of Direct Injection Stratified Charge Engines," *IEEE/ASME Trans. Mechatronics*, vol. 11, no. 5, pp. 499–506, 2006.

[8] P. Ortner and L. del Re, "Predictive Control of a Diesel Engine Air Path," *IEEE Trans. Contr. Systems Technology*, vol. 15, no. 3, pp. 449–456, 2007.

[9] G. Stewart and F. Borrelli, "A Model Predictive Control Framework for Industrial Turbodiesel Engine Control," in *Proc. 47th IEEE Conf. on Decision and Control*, Cancun, Mexico, Dec 2008, pp. 5704–5711.

[10] F. Borrelli, A. Bemporad, M. Fodor, and D. Hrovat, "An MPC/hybrid system approach to traction control," *IEEE Trans. Contr. Systems Technology*, vol. 14, no. 3, pp. 541–552, 2006.

[11] S. Di Cairano, H. E. Tseng, D. Bernardini, and A. Bemporad, "Vehicle yaw stability control by coordinated active front steering and differential braking in the tire sideslip angles domain," *IEEE Trans. Contr. Systems Technology*, vol. 21, no. 4, pp. 1236–1248, 2013.

[12] C. Beal and J. C. Gerdes, "Model predictive control for vehicle stabilization at the limits of handling," *IEEE Trans. Contr. Systems Technology*, vol. 21, no. 4, pp. 1258–1269, 2013.

[13] S. Di Cairano, W. Liang, I. V. Kolmanovsky, M. L. Kuang, and A. M. Phillips, "Power smoothing energy management and its application to a series hybrid powertrain," *IEEE Trans. Contr. Systems Technology*, vol. 21, no. 6, pp. 2091–2103, 2013.

[14] H. Borhan, A. Vahidi, A. M. Phillips, M. L. Kuang, I. V. Kolmanovsky, and S. Di Cairano, "Mpc-based energy management of a power-split hybrid electric vehicle," *IEEE Trans. Contr. Systems Technology*, vol. 20, no. 3, pp. 593–603, 2012.

[15] D. Hrovat, S. Di Cairano, H. Tseng, and I. Kolmanovsky, "The development of model predictive control in automotive industry: A survey," in *IEEE Int. Conf. Control Applications*, Dubrovnik, HR, 2012, pp. 295–302.
[16] S. Di Cairano, D. Yanakiev, A. Bemporad, I. Kolmanovsky, and D. Hrovat, "Model predictive idle speed control: Design, analysis, and experimental evaluation," *IEEE Trans. Contr. Systems Technology*, vol. 20, no. 1, pp. 84 –97, 2012.
[17] S. Di Cairano, J. Doering, I. Kolmanovsky, and D. Hrovat, "MPC based control of engine deceleration with open torque converter," in *Proc. 51th IEEE Conf. on Decision and Control*, Maui, HI, 2012, pp. 3753–3758.
[18] L. Guzzella and A. Sciarretta, *Vehicle Propulsion Systems Introduction to Modeling and Optimization*. Berlin Heidelberg, Germany: Springer Verlag, 2005.
[19] A. Lagerberg and B. Egardt, "Backlash estimation with application to automotive powertrains," *IEEE Trans. Contr. Systems Technology*, vol. 15, no. 3, pp. 483–493, 2007.
[20] D. Hrovat and J. Sun, "Models and control methodologies for IC engine idle speed control design," *Control Engineering Practice*, vol. 5, no. 8, pp. 1093 – 1100, 1997.
[21] J. B. Heywood, *Internal Combustion Engine Fundamentals*. New York, USA: McGraw-Hill, 1988.
[22] J. D. Powell, N. Fekete, and C.-F. Chang, "Observer-based air fuel ratio control," *IEEE Control Systems Magazine*, vol. 18, no. 5, pp. 72–83, 1998.
[23] A. Stotsky, B. Egardt, and S. Eriksson, "Variable structure control of engine idle speed with estimation of unmeasurable disturbances," *J. of Dynamic Systems, Meas. and Control*, vol. 122, pp. 599–603, 2000.
[24] D. Hrovat and W. Powers, "Modeling and control of automotive powertrains," *Control and Dynamic Systems*, vol. 37, pp. 33–64, 1990.
[25] G. Ferrari-Trecate, F. Cuzzola, D. Mignone, and M. Morari, "Analysis of discrete-time piecewise affine and hybrid systems," *Automatica*, vol. 38, pp. 2139–2146, 2002.
[26] K. Gu, J. Chen, and V. L. Kharitonov, *Stability of time delay systems*. Springer, 2003.
[27] B. J. Allison and A. J. Isaksson, "Design and performance of mid-ranging controllers," *J. Process Control*, vol. 8, no. 5, pp. 469–474, 1998.

Stefano Di Cairano (M'08) received the Master (Laurea), and the PhD in Information Engineering in 2004 and 2008, respectively, from the University of Siena, Italy. He was also granted the Int. Curr. Opt. of Doctoral Studies in Hybrid Control Systems. He was visiting student at the Technical University of Denmark, Lyngby, Denmark, in 2002–2003, and at the California Institute of Technology, Pasadena, CA, in 2006–2007. In 2008–2011, he was with Powertrain Control R&A, Ford Research and Adv. Engineering, Dearborn, MI. Since 2011 he is with the Mechatronics group of the Mitsubishi Electric Research Labs, Cambridge, MA, where he is now a Team Leader. His research is on advanced control strategies for complex mechatronic systems, in automotive, factory automation, and aerospace. His interests include model predictive control, constrained control, networked control systems, hybrid systems, optimization, automotive, aerospace, and factory automation.

Dr. Di Cairano is the Chair of the IEEE CSS Technical Committee on Automotive Controls, a member of the IEEE CSS Conference Editorial Board, and an Associate Editor of IEEE Trans. Control Systems Technology.

Jeff Doering received the B.S. in Aerospace Engineering from the University of Minnesota, Minneapolis, in 1991 and the M.S. in Mechanical Engineering from Stanford University in 1992. In 2000, Jeff received his Ph.D. in Mechanical Engineering from Michigan Technological University. Since 1992, he has been with Ford Motor Company, Dearborn, MI, working in the areas of engine and vehicle controls in both product development and research, where he is currently a Technical Leader in Research and Advanced Engineering.

Ilya Kolmanovsky has received his M.S. and Ph.D. degrees in aerospace engineering, and the M.A. degree in mathematics from the University of Michigan, Ann Arbor, in 1993, 1995, and 1995, respectively. He is presently a professor in the department of aerospace engineering at the University of Michigan with research interests in control theory for systems with state and control constraints, control of automotive and aerospace propulsion systems, and spacecraft control applications. Prior to joining the University of Michigan, Dr. Kolmanovsky was with Ford Research and Advanced Engineering in Dearborn, Michigan for close to 15 years. Dr. Kolmanovsky is a Fellow of IEEE, and a past recipient of the Donald P. Eckman Award of American Automatic Control Council, of IEEE Transactions on Control Systems Technology Outstanding Paper Award, and several Ford Research and Advanced Engineering Technical Achievement, Innovation and Publication awards.

Davor Hrovat received his B.Sc.M.E. (Dipl. Ing.) degree from the University of Zagreb, Croatia in 1972, and his M.Sc. and Ph.D. degrees in Mechanical Engineering from the University of California, Davis in 1976 and 1979, respectively. Since 1981, he has been with the Ford Research Laboratory (FRL) in Dearborn, Michigan. At FRL, he is a Henry Ford Technical Fellow, coordinating and leading research efforts on various aspects of vehicle/power train control systems, where he holds numerous patents. He has served on editorial boards for a number of ASME and IEEE journals, and is currently an Editor for the IFAC journal Control Engineering Practice, and the International Journal of Vehicle Autonomous Systems. Dr. Hrovat is a Fellow of the American Society of Mechanical Engineers (ASME) and also a Fellow of the Institute of Electrical and Electronics Engineers (IEEE). He is the recipient of the 1996 ASME/Dynamic Systems and Control Innovative Practice Award and the 1999 AACC Control Engineering Practice Award. He is a member of the National Academy of Engineering.